PHYSICAL REVIEW B **96**, 041101(R) (2017)

Landau-level spectroscopy of massive Dirac fermions in single-crystalline $ZrTe_5$ thin flakes

Y. Jiang,[1] Z. L. Dun,[2] H. D. Zhou,[2] Z. Lu,[3,4] K.-W. Chen,[3,4] S. Moon,[3,4] T. Besara,[3]
T. M. Siegrist,[3,5] R. E. Baumbach,[3] D. Smirnov,[3] and Z. Jiang[1,*]

[1]*School of Physics, Georgia Institute of Technology, Atlanta, Georgia 30332, USA*
[2]*Department of Physics and Astronomy, University of Tennessee, Knoxville, Tennessee 37996, USA*
[3]*National High Magnetic Field Laboratory, Tallahassee, Florida 32310, USA*
[4]*Department of Physics, Florida State University, Tallahassee, Florida 32306, USA*
[5]*Department of Chemical and Biomedical Engineering, Florida A&M University–Florida State University (FAMU-FSU) College of Engineering, Florida State University, Tallahassee, Florida 32310, USA*

(Received 27 March 2017; published 5 July 2017)

We report infrared magnetospectroscopy studies on thin crystals of an emerging Dirac material $ZrTe_5$ near the intrinsic limit. The observed structure of the Landau-level transitions and zero-field infrared absorption indicate a two-dimensional Dirac-like electronic structure, similar to that in graphene but with a small relativistic mass corresponding to a 9.4-meV energy gap. Measurements with circularly polarized light reveal a significant electron-hole asymmetry, which leads to splitting of the Landau-level transitions at high magnetic fields. Our model, based on the Bernevig-Hughes-Zhang effective Hamiltonian, quantitatively explains all observed transitions, determining the values of the Fermi velocity, Dirac mass (or gap), electron-hole asymmetry, and electron and hole g factors.

DOI: 10.1103/PhysRevB.96.041101

Zirconium pentatelluride ($ZrTe_5$) has long been recognized as a layered thermoelectric material [1]. It has attracted substantial interest lately in the wave of Dirac and topological material exploration [2] due to the theoretical prediction of a large-gap quantum spin Hall insulator phase in its monolayer form [3]. Theory also predicts that the electronic structure of bulk $ZrTe_5$ resides near the phase boundary between weak and strong topological insulators (TIs) [3,4], providing an ideal platform for studying topological phase transitions. Surface-sensitive spectroscopy techniques such as angle-resolved photoemission spectroscopy (ARPES) and scanning tunneling spectroscopy have recently been used to probe the surface and bulk states of $ZrTe_5$ [5–11]. Intriguingly, results from different groups lead to conflicting interpretations ranging from strong/weak TI [6–9,11] to Dirac semimetal [5,10].

On the other hand, infrared (IR) spectroscopy is a bulk-sensitive technique. Recent IR reflectance studies have suggested that bulk $ZrTe_5$ is a three-dimensional (3D) massless Dirac semimetal [12–14]. However, the accuracy of the transition energies extracted from the reflectance measurements may be questioned as their positions are not necessarily aligned with particular spectral peaks or dips [15]. Therefore, magneto-IR transmission measurements are needed to quantitatively describe the exact topological nature of $ZrTe_5$.

In this Rapid Communication, we present the IR transmission magnetospectroscopy study of mechanically exfoliated $ZrTe_5$ thin crystals near the intrinsic limit. Because of the low carrier density, we are able to observe a series of interband Landau-level (LL) transitions that exhibit the characteristic dispersion of two-dimensional (2D) massive Dirac fermions—a signature of the 2D Dirac semimetal electronic structure. We employ high-field magnetospectroscopy with circularly polarized IR light to resolve a fourfold splitting of low-lying LL transitions, which is attributed to the combined effect of finite mass, large g factor, and electron-hole asymmetry.

$ZrTe_5$ single crystals were prepared by the Te-assisted chemical vapor transport (CVT) method [16] or molten Te flux growth [5]. The crystal has a layered structure with weakly van der Waals coupled layers along the b axis [Fig. 1(a)]. By repeatedly exfoliating the material with an IR-transparent Scotch tape, we prepared thin $ZrTe_5$ flakes with an average thickness of about 1 μm that enables IR transmission/absorption measurements. This method has been proven successful in previous studies of graphite [17,18] and TI materials such as Bi_2Te_3 [19]. In the main text below, we present the data taken on CVT-grown samples. Similar results were measured with the flux-grown samples, as reported in the Supplemental Material [20] together with a detailed description of the crystal growth and experimental setup.

In Fig. 1(b), we plot the zero-field extinction spectrum, $1 - T/T_{\text{tape}}$, of $ZrTe_5$/tape composite measured at 25 K. Here, the sample spectrum (T) is referenced to the transmission through a bare tape (T_{tape}). At low photon energies, the extinction coefficient, and consequently, the absorption (A) first increases with energy (E) and then becomes spectrally flat at $E > 75$ meV. This behavior clearly deviates from the expected linear dependence, $A \propto E$, for 3D Dirac semimetals [21] and differentiates our thin flake samples from the thick, opaque samples studied in Refs. [12,13], where a 3D massless Dirac semimetal electronic structure was concluded for $ZrTe_5$. Moreover, our data are similar to that observed in graphene [22,23], the best known material system hosting 2D Dirac fermions, for the entire experimental spectral range. Due to its 2D nature, $A = const.$ in mono-, bi-, and multilayer graphene at high photon energies [24–27]. This 2D Dirac fermion speculation is supported by recent transport studies on $ZrTe_5$ thin flakes [14,28–30].

*zhigang.jiang@physics.gatech.edu

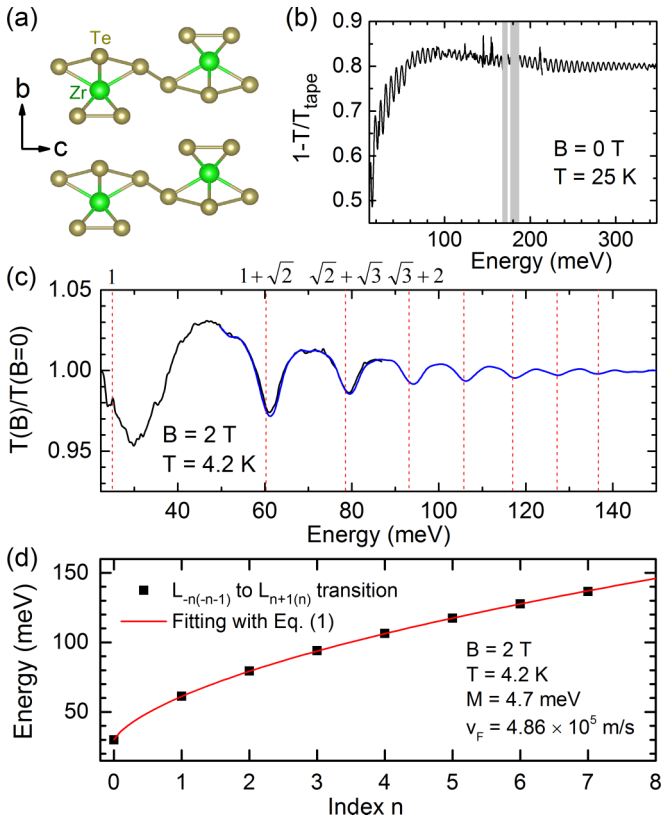

FIG. 1. (a) Schematic view of $ZrTe_5$ unit cell along the a axis. The layer stacking direction is along the b axis. (b) Extinction spectrum, $1 - T/T_{\text{tape}}$, of $ZrTe_5$/tape composite measured at $B = 0$ T and $T = 25$ K. The fast oscillations originate from the Fabry-Pérot interference. The gray stripes cover the opaque regions due to tape absorption. (c) Normalized transmission spectrum, $T(B)/T(B = 0)$, measured at $B = 2$ T and $T = 4.2$ K. The black and blue curves correspond to the far-IR and the mid-IR spectrum, respectively. The red dashed lines mark the expected energies of $L_{-n(-n-1)} \rightarrow L_{n+1(n)}$ transitions for massless Dirac fermions. (d) Extracted LL transition energy from (c) as a function of LL index n. The red line shows the best fit to the data using Eq. (1).

To elucidate the electronic structure of $ZrTe_5$ thin flakes, we carry out systematic low-temperature IR transmission measurements in the Faraday geometry in magnetic fields up to $B = 16$ T. Figure 1(c) shows a normalized transmission spectrum taken at $B = 2$ T featuring a characteristic, graphenelike series of absorption minima. Indeed, the transition energies, which can be readily and accurately determined from the central energy of the absorption line, can be assigned to a series of interband LL transitions from $L_{-n(-n-1)}$ to $L_{n+1(n)}$ with the integer n (or $-n$) being the LL index. The LL spectrum of 2D Dirac fermions such as that in graphene can be described as

$$E_n = \alpha\sqrt{2e\hbar v_F^2 nB + M^2}, \tag{1}$$

where E_n is the energy of the nth LL, e is the electron charge, $\hbar$ is the reduced Planck's constant, v_F is the Fermi velocity, M is the Dirac mass, and $\alpha = \pm 1$ stands for the conduction and valence bands, respectively. For massless Dirac fermions, $E_n \propto \sqrt{n}$, leading to the characteristic $E_{-n\rightarrow n+1} \propto \sqrt{n} + \sqrt{n+1}$ dependence of optically allowed interband LL transitions $L_{-n} \rightarrow L_{n+1}$ [31,32]. For massive Dirac fermions ($M \neq 0$), however, E_n deviates from a perfect $\sqrt{n}$ dependence [33]. The deviation becomes more pronounced for low-lying LL transitions when n is small. Such a massive Dirac fermion scenario can precisely describe our data at low magnetic fields. The vertical dashed lines in Fig. 1(c) indicate transition energies following a model $\sqrt{n} + \sqrt{n+1}$ dependence, with the parameter v_F determined by the highest energy transition ($n = 7$). The measured energies of LL transitions exhibit a clear blueshift, particularly for low-lying transitions, suggesting the massive Dirac fermion interpretation. A more quantitative analysis is shown in Fig. 1(d), where the extracted transition energies are plotted as a function of n and fitted with Eq. (1). The best fit to the data gives $M = 4.7$ meV (corresponding to a 9.4 meV energy gap) and $v_F = 4.86 \times 10^5$ m/s. The latter is the average Fermi velocity in the ac plane of $ZrTe_5$ and its value is consistent with recent transport [34], ARPES [11], and IR [13] measurements.

The observation of a small Dirac mass of $M = 4.7$ meV is not a surprise. In theory, the Dirac point in semimetals such as $ZrTe_5$ is composed of two overlapping Weyl points with opposite chirality [35–37]. When it lacks symmetry protection, the annihilation of the Weyl points leads to a gap opening at the Dirac point, equivalent to generating a Dirac mass. In addition, the lowest energy transition observed is $L_{0(-1)} \rightarrow L_{1(0)}$, which implies that our sample is in quantum limit. This transition is visible at the magnetic field as low as 0.5 T, corresponding to a Fermi energy $\leqslant$16 meV. Therefore, our samples are close to the intrinsic limit, suited for magneto-IR spectroscopy studies. Also, we note that the Lorentzian line shape of LL transitions [Fig. 1(c)] provides another indication in favor of a 2D Dirac fermion picture, as the k_z dispersion in a 3D system would lead to an asymmetric line shape with abrupt cutoff on the low-energy side [38].

Figure 2(a) illustrates the magnetic field dependence of the LL transitions and their splitting in high magnetic fields, particularly for the three lowest interband transitions: $L_{0(-1)} \rightarrow L_{1(0)}$, $L_{-1(-2)} \rightarrow L_{2(1)}$, and $L_{-2(-3)} \rightarrow L_{3(2)}$. The splitting of the $L_{0(-1)} \rightarrow L_{1(0)}$ transition was previously observed in magneto-IR reflectance measurements [13], but the proposed interpretation suffers from the requirement of two sets of g factors. In this work, to explore the origins of the splitting, we performed magneto-IR circular polarization resolved measurements using mid-IR quantum cascade lasers (QCLs) [20]. Magnetospectroscopy with circularly polarized light has been successfully employed in the past to reveal details of specific LL transitions in graphite [39], and more recently in graphene [40] and in a typical 3D TI Bi_2Se_3 [41]. Here, we focus on the $L_{-1(-2)} \rightarrow L_{2(1)}$ transition, which overlaps well the spectral range of our QCLs. The circular polarization resolved spectra are taken by fixing the light polarization and sweeping the magnetic field in positive or negative directions, which is equivalent to the use of σ^+ and σ^- polarized light.

Figure 3 shows the normalized transmission through $ZrTe_5$/tape composite as a function of magnetic field with the QCL energy fixed at $E_{QCL} = 117$ meV. With unpolarized

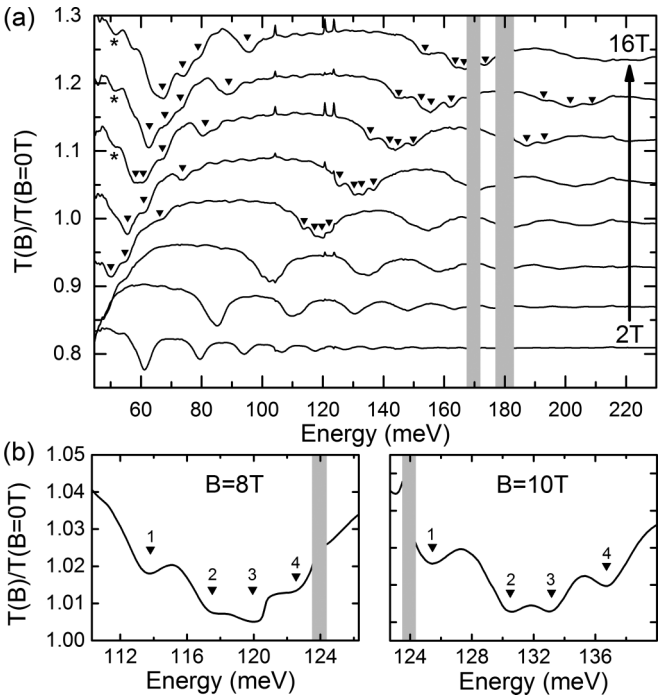

FIG. 2. (a) Normalized transmission spectra, $T(B)/T(B=0\ \mathrm{T})$, of $ZrTe_5$/tape composite measured at selected magnetic fields. The down triangles (▼) label the splitting of low-lying LL transitions, while the star symbols (⋆) point to B-independent spectral features originating from the normalization process. (b) Zoom-in view of the fourfold splitting of the $L_{-1(-2)} \rightarrow L_{2(1)}$ transition taken at $B = 8$ T and 10 T. In all panels, the spectra are offset vertically for clarity, and the gray stripes cover the opaque regions due to tape absorption.

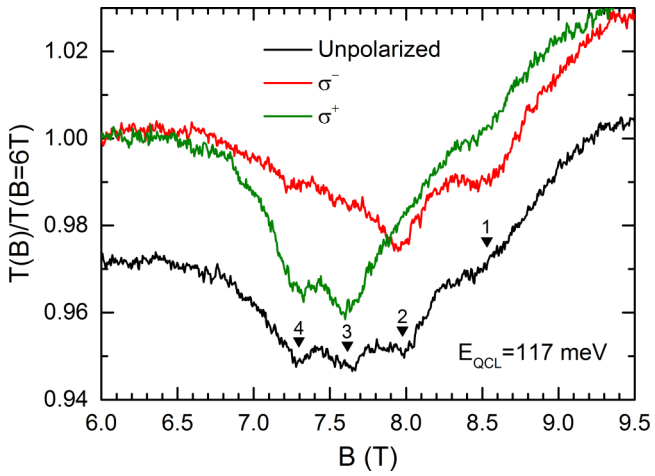

FIG. 3. Normalized transmission, $T(B)/T(B=6\ \mathrm{T})$, through $ZrTe_5$/tape composite as a function of magnetic field with unpolarized (black) and circularly polarized (red and green) incident IR light of 117 meV. The negative magnetic field sweep (green) is flipped to the positive side for ease of comparison. The fourfold splitting of the $L_{-1(-2)} \rightarrow L_{2(1)}$ transition is labeled by down triangles (▼) on the unpolarized data, which is offset vertically for clarity.

IR light, a fourfold splitting of the $L_{-1(-2)} \rightarrow L_{2(1)}$ transition clearly reproduces that measured at $B = const$. [Fig. 2(b)]. In a circularly polarized configuration, only two of the four split transitions are active in σ^+ or σ^- polarized light. This observation indicates the lifting of the degeneracy between the $L_{-1} \rightarrow L_2$ ($\Delta n = 1, \sigma^+$ active) and $L_{-2} \rightarrow L_1$ ($\Delta n = -1, \sigma^-$ active) transitions, which can be attributed to an asymmetry between the electron and hole bands.

Next, we show that the remaining twofold splitting of the $L_{-1} \rightarrow L_2$ (or $L_{-2} \rightarrow L_1$) transition reflects the lifting of the spin degeneracy, due to a combined effect of large g factor (Zeeman effect) and finite mass. We begin with an effective Hamiltonian postulated by Bernevig *et al.* [42],

$$H(\mathbf{k}) = \epsilon_0(\mathbf{k}) + \begin{pmatrix} L(\mathbf{k}) & Ak_+ & 0 & 0 \\ Ak_- & -L(\mathbf{k}) & 0 & 0 \\ 0 & 0 & L(\mathbf{k}) & -Ak_- \\ 0 & 0 & -Ak_+ & -L(\mathbf{k}) \end{pmatrix},$$

where $\epsilon_0(\mathbf{k}) = C - D(k_x^2 + k_y^2)$, $L(\mathbf{k}) = M - \mathscr{B}(k_x^2 + k_y^2)$, $k_\pm = k_x \pm ik_y$, and k^4 terms neglected [37]. The actual electronic structure is then determined by a set of material parameters: (1) $A = \hbar v_F$, (2) band inversion parameter $\mathscr{B}$, (3) energy offset C (which is set to zero), (4) electron-hole asymmetry parameter D, and (5) Dirac mass M. In the presence of a magnetic field, one can add the Zeeman term [43,44], $\frac{\mu_B B}{2}\begin{pmatrix} g & 0 \\ 0 & -g \end{pmatrix}$, where μ_B is the Bohr magneton, $g = \begin{pmatrix} g_e & 0 \\ 0 & g_h \end{pmatrix}$, and $g_e(g_h)$ are the effective g factors for conduction (valence) bands and solve the eigenvalue problem for the LL spectrum of massive Dirac fermions in $ZrTe_5$ thin flakes:

$$E_0^{\uparrow} = M - (D + \mathscr{B})\frac{eB}{\hbar} + \frac{\mu_B g_e}{2}B, \quad E_0^{\downarrow} = -M - (D - \mathscr{B})\frac{eB}{\hbar} - \frac{\mu_B g_h}{2}B, \quad n = 0, \tag{2}$$

$$E_{n,\alpha}^{s} = -(2Dn + s\mathscr{B})\frac{eB}{\hbar} + s\frac{\mu_B \bar{Z}}{2}B + \alpha\sqrt{2A^2 n\frac{eB}{\hbar} + \left[M - (2\mathscr{B}n + sD)\frac{eB}{\hbar} + s\frac{\mu_B \delta Z}{2}B\right]^2}, \quad n \neq 0. \tag{3}$$

Here, $s = \uparrow\downarrow = \pm 1$ stands for the spin-up and spin-down LLs, $\bar{Z} = \frac{g_e + g_h}{2}$ is the average g factor, and $\delta Z = \frac{g_e - g_h}{2}$. In the low-field limit, Eqs. (2) and (3) reduce to Eq. (1). It should be emphasized that the Zeeman effect alone cannot lift the spin degeneracy of LL transitions, even when considering electron-hole asymmetry, $D \neq 0$ and $\delta Z \neq 0$. This can be seen in Eq. (3), where a finite mass, $M \neq 0$ and/or $\mathscr{B} \neq 0$ [45], is required to distinguish the $[\cdots]^2$ term for $s = \pm 1$. Therefore, the observed fourfold splitting of low-lying LL transitions provides another evidence of finite mass for the Dirac fermions in $ZrTe_5$ thin flakes.

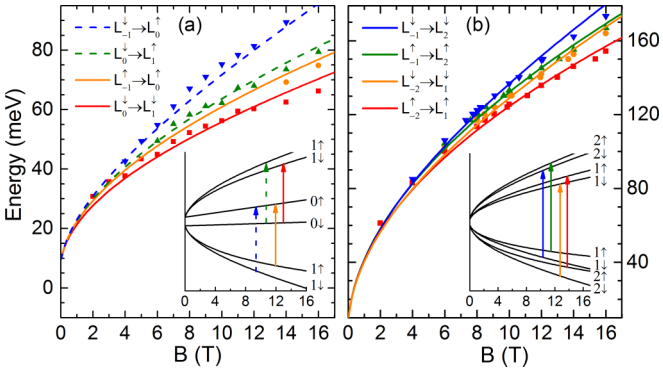

FIG. 4. Fourfold splitting of the (a) $L_{0(-1)} \rightarrow L_{1(0)}$ and (b) $L_{-1(-2)} \rightarrow L_{2(1)}$ transitions as a function of magnetic field. Symbols represent the extracted transition energies from both the broad-band measurements at constant magnetic field and the QCL-based measurements at constant photon energy [20]. The color-coded lines show best fits to the data using Eqs. (2) and (3). The corresponding transitions are illustrated in the insets with the same color code. The solid and dashed lines denote the spin-conserved strong transitions and the spin-flipped weak transitions, respectively.

Figure 4(b) shows the fourfold splitting of the $L_{-1(-2)} \rightarrow L_{2(1)}$ transition as a function of magnetic field and the color-coded lines are best fits to the data using Eq. (3). The associated fitting parameters are $v_F = 4.65 \times 10^5$ m/s, $\mathscr{B} = 341$ meV nm^2, $D = -126$ meV nm^2, $M = 4.71$ meV, $g_e = 24.3$, and $g_h = 7.5$. Here, M is consistent with that obtained from Fig. 1(d) while v_F is ~4% smaller, and $D < 0$ implies a steeper conduction band than the valence band. Interestingly, we notice that a smaller v_F is also needed to better describe the high-field data in Ref. [43].

To further validate our model, we checked if the above parameters allow us to describe other split transitions and found a very good agreement for the $L_{0(-1)} \rightarrow L_{1(0)}$ transition [Fig. 4(a)]. Due to the strong spin-orbit coupling in $ZrTe_5$, spin-flipped LL transitions ($L_0^{\downarrow} \rightarrow L_1^{\uparrow}$ and $L_{-1}^{\downarrow} \rightarrow L_0^{\uparrow}$) are allowed and assigned to the two relatively weak high-energy modes of the $L_{0(-1)} \rightarrow L_{1(0)}$ splitting. The fourfold splitting of the $L_{-1(-2)} \rightarrow L_{2(1)}$ transition, on the other hand, is related to the four strong spin-conserved modes, as the associated spin-flipped modes are expected to be very weak.

Lastly, our model predicts that additional splitting of the $L_{0(-1)} \rightarrow L_{1(0)}$ transition into $L_0^{\uparrow} \rightarrow L_1^{\uparrow}$ ($L_{-1}^{\downarrow} \rightarrow L_0^{\downarrow}$) may occur at lower energies due to the presence of a small amount of electron (hole) doping. Quantitative study of this mode, however, is hindered by a field-independent spectral feature at ~52 meV [labeled by star symbol in Fig. 2(a)] and thus is not pursued in this work.

In conclusion, we have performed IR transmission measurements on exfoliated $ZrTe_5$ near the intrinsic limit. The electronic structure of $ZrTe_5$ thin crystals is found to be 2D-like and supports a Dirac semimetal interpretation but with a small relativistic mass (or gap). High-field magnetospectroscopy measurements reveal a fourfold splitting of low-lying LL transitions, and circular-polarization-resolved measurements show that twofold comes from breaking the electron-hole symmetry while the other twofold is caused by lifting the spin degeneracy. The magnetic field dependence of the splitting can be fully described using the Bernevig-Hughes-Zhang effective Hamiltonian model.

Note added. Recently we became aware of another IR transmission study of $ZrTe_5$ thin flake [46].

We thank Kun Yang and Markus Kindermann for helpful discussions. This work was primarily supported by the DOE (Grant No. DE-FG02-07ER46451). The CVT crystal growth at UT was supported by the NSF (Grant No. DMR-1350002). The flux crystal growth and IR measurements were performed at the National High Magnetic Field Laboratory (NHMFL), which is supported by NSF Cooperative Agreement No. DMR-1157490 and the State of Florida. Z.J. acknowledges support from the NHMFL Visiting Scientist Program.

[1] R. T. Littleton IV, T. M. Tritt, C. R. Feger, J. Kolis, M. L. Wilson, M. Marone, J. Payne, D. Verebeli, and F. Levy, Appl. Phys. Lett. **72**, 2056 (1998).

[2] O. Vafek and A. Vishwanath, Annu. Rev. Condens. Matter Phys. **5**, 83 (2014).

[3] H. M. Weng, X. Dai, and Z. Fang, Phys. Rev. X **4**, 011002 (2014).

[4] Z. Fan, Q.-F. Liang, Y. B. Chen, S.-H. Yao, and J. Zhou, Sci. Rep. **7**, 45667 (2017).

[5] Q. Li, D. E. Kharzeev, C. Zhang, Y. Huang, I. Pletikosić, A. V. Fedorov, R. D. Zhong, J. A. Schneeloch, G. D. Gu, and T. Valla, Nat. Phys. **12**, 550 (2016).

[6] R. Wu, J.-Z. Ma, S.-M. Nie, L.-X. Zhao, X. Huang, J.-X. Yin, B.-B. Fu, P. Richard, G.-F. Chen, Z. Fang *et al.*, Phys. Rev. X **6**, 021017 (2016).

[7] X.-B. Li, W.-K. Huang, Y.-Y. Lv, K.-W. Zhang, C.-L. Yang, B.-B. Zhang, Y. B. Chen, S.-H. Yao, J. Zhou, M.-H. Lu *et al.*, Phys. Rev. Lett. **116**, 176803 (2016).

[8] L. Moreschini, J. C. Johannsen, H. Berger, J. Denlinger, C. Jozwiak, E. Rotenberg, K. S. Kim, A. Bostwick, and M. Grioni, Phys. Rev. B **94**, 081101(R) (2016).

[9] G. Manzoni, L. Gragnaniello, G. Autès, T. Kuhn, A. Sterzi, F. Cilento, M. Zacchigna, V. Enenkel, I. Bobornik, L. Barba *et al.*, Phys. Rev. Lett. **117**, 237601 (2016).

[10] L. Shen *et al.*, J. Electron Spectrosc. Relat. Phenom. doi:10.1016/j.elspec.2016.10.007.

[11] Y. Zhang *et al.*, Nat. Commun. **8**, 15512 (2017).

[12] R. Y. Chen, S. J. Zhang, J. A. Schneeloch, C. Zhang, Q. Li, G. D. Gu, and N. L. Wang, Phys. Rev. B **92**, 075107 (2015).

[13] R. Y. Chen, Z. G. Chen, X.-Y. Song, J. A. Schneeloch, G. D. Gu, F. Wang, and N. L. Wang, Phys. Rev. Lett. **115**, 176404 (2015).

[14] X. Yuan *et al.*, NPG Asia Mater. **8**, e325 (2016).

[15] A. Akrap, M. Hakl, S. Tchoumakov, I. Crassee, J. Kuba, M. O. Goerbig, C. C. Homes, O. Caha, J. Novák, F. Teppe *et al.*, Phys. Rev. Lett. **117**, 136401 (2016).

[16] *Chemical Vapor Transport Reactions*, edited by M. Binnewies, R. Glaum, M. Schmidt, and P. Schmidt (Walter de Gruyter, Berlin, 2012).
[17] M. Orlita, C. Faugeras, G. Martinez, D. K. Maude, M. L. Sadowski, and M. Potemski, Phys. Rev. Lett. **100**, 136403 (2008).
[18] K.-C. Chuang, A. M. R. Baker, and R. J. Nicholas, Phys. Rev. B **80**, 161410(R) (2009).
[19] L.-C. Tung, W. Yu, P. Cadden-Zimansky, I. Miotkowski, Y. P. Chen, D. Smirnov, and Z. Jiang, Phys. Rev. B **93**, 085140 (2016).
[20] See Supplemental Material at http://link.aps.org/supplemental/10.1103/PhysRevB.96.041101 for crystal synthesis and experimental details, additional experimental data, and extended effective Hamiltonian model.
[21] T. Timusk, J. P. Carbotte, C. C. Homes, D. N. Basov, and S. G. Sharapov, Phys. Rev. B **87**, 235121 (2013).
[22] K. F. Mak, M. Y. Sfeir, Y. Wu, C. H. Lui, J. A. Misewich, and T. F. Heinz, Phys. Rev. Lett. **101**, 196405 (2008).
[23] Z. Q. Li, E. A. Henriksen, Z. Jiang, Z. Hao, M. C. Martin, P. Kim, H. L. Stormer, and D. N. Basov, Nat. Phys. **4**, 532 (2008).
[24] N. M. R. Peres, F. Guinea, and A. H. Castro Neto, Phys. Rev. B **73**, 125411 (2006).
[25] D. S. L. Abergel and V. I. Fal'ko, Phys. Rev. B **75**, 155430 (2007).
[26] S. Ryu, C. Mudry, A. Furusaki, and A. W. W. Ludwig, Phys. Rev. B **75**, 205344 (2007).
[27] M. Koshino and T. Ando, Phys. Rev. B **77**, 115313 (2008).
[28] W. Yu, Y. Jiang, J. Yang, Z. L. Dun, H. D. Zhou, Z. Jiang, P. Lu, and W. Pan, Sci. Rep. **6**, 35357 (2016).
[29] Y. W. Liu *et al.*, Nat. Commun. **7**, 12516 (2016).
[30] J. J. Niu, J. Y. Wang, Z. J. He, C. L. Zhang, X. Q. Li, T. C. Cai, X. M. Ma, S. Jia, D. P. Yu, and X. S. Wu, Phys. Rev. B **95**, 035420 (2017).
[31] M. L. Sadowski, G. Martinez, M. Potemski, C. Berger, and W. A. de Heer, Phys. Rev. Lett. **97**, 266405 (2006).
[32] Z. Jiang, E. A. Henriksen, L.-C. Tung, Y.-J. Wang, M. E. Schwartz, M. Y. Han, P. Kim, and H. L. Stormer, Phys. Rev. Lett. **98**, 197403 (2007).
[33] Z.-G. Chen, Z. W. Shi, W. Yang, X. B. Lu, Y. Lai, H. G. Yan, F. Wang, G. Y. Zhang, and Z. Q. Li, Nat. Commun. **5**, 4461 (2014).
[34] G. L. Zheng, J. Lu, X. Zhu, W. Ning, Y. Han, H. Zhang, J. Zhang, C. Xi, J. Yang, H. Du, K. Yang, Y. Zhang, and M. Tian, Phys. Rev. B **93**, 115414 (2016).
[35] J. L. Mañes, Phys. Rev. B **85**, 155118 (2012).
[36] S. M. Young, S. Zaheer, J. C. Y. Teo, C. L. Kane, E. J. Mele, and A. M. Rappe, Phys. Rev. Lett. **108**, 140405 (2012).
[37] Z. J. Wang, Y. Sun, X. Q. Chen, C. Franchini, G. Xu, H. M. Weng, X. Dai, and Z. Fang, Phys. Rev. B **85**, 195320 (2012); Z. J. Wang, H. M. Weng, Q. S. Wu, X. Dai, and Z. Fang, *ibid.* **88**, 125427 (2013).
[38] M. Orlita *et al.*, J. Appl. Phys. **117**, 112803 (2015).
[39] W. W. Toy, M. S. Dresselhaus, and G. Dresselhaus, Phys. Rev. B **15**, 4077 (1977).
[40] I. Crassee, J. Levallois, D. van der Marel, A. L. Walter, Th. Seyller, and A. B. Kuzmenko, Phys. Rev. B **84**, 035103 (2011).
[41] M. Orlita, B. A. Piot, G. Martinez, N. K. Sampath Kumar, C. Faugeras, M. Potemski, C. Michel, E. M. Hankiewicz, T. Brauner, C. Drašar *et al.*, Phys. Rev. Lett. **114**, 186401 (2015).
[42] B. A. Bernevig, T. L. Hughes, and S.-C. Zhang, Science **314**, 1757 (2006).
[43] B. Büttner *et al.*, Nat. Phys. **7**, 418 (2011).
[44] J. Ludwig, Y. B. Vasilyev, N. N. Mikhailov, J. M. Poumirol, Z. Jiang, O. Vafek, and D. Smirnov, Phys. Rev. B **89**, 241406(R) (2014).
[45] The parameter $\mathscr{B}$ can also be viewed as a field-induced mass.
[46] Z.-G. Chen *et al.*, Proc. Natl. Acad. Sci. USA **114**, 816 (2017).